Journal of Power Sources 653 (2025) 237568

Contents lists available at ScienceDirect

Journal of Power Sources

journal homepage: www.elsevier.com/locate/jpowsour

TinyML models for SoH estimation of lithium-ion batteries based on Electrochemical Impedance Spectroscopy☆,☆☆

Spyridon Giazitzis [a,*], Abdisamad Ahmed Isse [b], Nicola Blasuttigh [b], Alessandro Massi Pavan [b], Davide M. Raimondo [b], Susheel Badha [c], Filippo Rosetti [c], Emanuele Ogliari [a]

[a] Politecnico di Milano, Department of Energy, Via Lambruschini, 8, 20156, Milan, Italy
[b] Department of Engineering and Architecture, and Center for Energy, Environment and Transport Giacomo Ciamician, University of Trieste, Trieste, Italy
[c] Infineon Technologies, Siemensstraße 2, Villach, 9500, Austria

HIGHLIGHTS

- Developed TinyML models for battery SoH estimation from EIS data.
- Compared ECM-based and raw EIS data-driven approaches for model development.
- Optimized models converted to TinyML for real-time edge device deployment.
- CNN-GRU model achieved highest performance by using raw EIS data.

ARTICLE INFO

Keywords:
Electrochemical impedance spectroscopy
State of health
Deep learning models
Batteries
TinyML
Equivalent Circuit Model (ECM)

ABSTRACT

As battery systems become more widespread, the need for accurate and fast estimation of State of Health (SoH) in lithium-ion cells is increasingly critical. This study analyzes two data-driven model methods that leverage Electrochemical Impedance Spectroscopy (EIS) measurements to capture the internal electrochemical dynamics underlying battery degradation and estimate the cell's current SoH. The first approach, Method A, utilizes an Equivalent Circuit Model (ECM) from EIS data and uses it to train various state-of-the-art Deep Learning (DL) models, including LSTM, GRU, CNN-LSTM, and CNN-GRU. In contrast, Method B directly employs raw EIS data to train the same set of DL models, bypassing the need for ECM development. Both methods demonstrated strong performance, with the CNN-GRU model from Method B yielding the best results, achieving a Mean Absolute Error (MAE) of only 0.87% and a Root Mean Square Error (RMSE) of 1.20%. Additionally, both methods included an analysis of various input features, such as State of Charge (SoC), to evaluate their impact on model performance. Finally, the models of Method B were optimized for size and computational efficiency, making them suitable for deployment on low-power edge devices and applications requiring TinyML capabilities. The average latency and size reduction of the models were 99.61% and 88.61%, respectively.

1. Introduction

As the world accelerates its transition towards sustainable energy, the role of Battery Energy Storage Systems (BESS) has become increasingly pivotal. These systems are integrated into several sectors, including automotive, industrial applications, and electrical grids, serving as support for improvement of energy efficiency and grid stability [1]. By optimizing energy use and facilitating the integration of renewable sources, BESS reduce dependence on fossil fuels and lower greenhouse gas emissions, contributing to a more sustainable energy system. Additionally, they enable the provision of ancillary services that enhance grid stability through advanced control systems [2]. To fully exploit the potential of BESS, an effective Battery Management System (BMS) is essential. A well-designed BMS ensures safe and efficient operation by accurately assessing cell conditions, monitoring and balancing charge levels, detecting faults, managing thermal conditions, and ensuring

☆ This study was carried out within the MOST — Sustainable Mobility Center and received funding from the European Union Next-GenerationEU (PIANO NAZIONALE DI RIPRESA E RESILIENZA (PNRR) – MISSIONE 4 COMPONENTE 2, INVESTIMENTO 1.4 – D.D. 1033 17/06/2022, CN00000023). This manuscript reflects only the authors' views and opinions, neither the European Union nor the European Commission can be considered responsible for them.
☆☆ This work was partially supported by the European Union through the EcoMobility project (grant 101112306)
* Corresponding author.
E-mail address: spyridon.giazitzis@polimi.it (S. Giazitzis).

https://doi.org/10.1016/j.jpowsour.2025.237568
Received 4 March 2025; Received in revised form 8 May 2025; Accepted 2 June 2025
Available online 24 June 2025

overall system safety. These functions are critical for enhancing the lifespan, reliability, and overall performance of the BESS [3].

Batteries degrade over time due to repeated charge–discharge cycles, temperature fluctuations, and natural aging processes, resulting in an increase of internal resistance and a gradual loss of capacity and overall performance. Without proper monitoring, this deterioration can lead to unexpected failures, reduced efficiency, and increased safety risks. For this reason, accurate and rapid estimation of the State of Health (SoH) is crucial. Several experimental approaches such as acoustic sensing [4], thermal analysis [5], gas evolution monitoring [6], and strain or pressure sensing [7] have been proposed to assess battery health by relying on directly measurable physical signals. Among these, Electrochemical Impedance Spectroscopy (EIS) stands out as a particularly powerful and non-destructive technique, capable of capturing detailed information about internal resistance, capacitive behavior, and diffusion processes, which are all key indicators of battery degradation [8]. EIS tests utilize a small-amplitude AC excitation signal to ensure linearity between the perturbation signal and the system's response, while minimizing stress on the battery cell. These tests typically take only a few seconds or minutes to complete [9]. For further details, in Section 2.2 there is an in-depth analysis of the applications and modes of EIS. This rapid assessment is essential for real-life applications that require fast diagnostics and prognostics, such as the repair of EVs, Uninterruptible Power Supply (UPS), and other critical BESS.

Methods utilizing EIS data for SoH estimation can be broadly classified into two main categories, the mathematical function based approach and data-driven modeling approach. In the literature, as shown in the following sections, both methods can leverage the parameters of an Equivalent Circuit Model (ECM) to enhance their performance and impose physical constraints on the models. ECM parameters can offer valuable insights into the degradation stage of a battery cell, reflecting phenomena such as capacity fade and increases in internal resistance. These parameters can be utilized to develop empirical or semi-empirical mathematical models that approximate the cell's SoH. Therefore, these parameters should be regularly updated to ensure reliable performance.

In mathematical function approaches, researchers derive mathematical equations from previous degradation experiments and develop or utilize predefined functions, often polynomials of second order or higher, to achieve accurate SoH estimation while accounting for factors such as temperature, resistances, and State of Charge (SoC). A notable contribution by [10] presents a fast and efficient method for estimating the SoH of lithium-ion batteries (LIBs) using partial EIS measurements, rather than utilizing data from the entire frequency range. By utilizing the real part of impedance at two specific frequencies, this method drastically reduces measurement time from 30 min to just 3 min while maintaining accurate SoH predictions through a second-order fitting function.

Similarly, [11] analyzed EIS data from four battery cells across different SoC levels, temperatures, and degradation stages, tracking their evolution up to End of Life (EOL) defined by a 20% capacity fade. Using these data, an ECM is developed, incorporating solid electrolyte interface (SEI) and charge transfer resistances to characterize their relationship with battery's degradation stage, under varying temperatures and SoC. A probabilistic model for SoH estimation is then formulated, utilizing charge transfer resistance, temperature, and SoC as input variables.

In [12], the Distribution of Relaxation Times (DRT) was employed to extract indicators associated with degradation modes, capturing various aging mechanisms. These indicators were used to simulate aging progression throughout the battery's lifetime, enabling SoH estimation. Two logarithmic decay functions were developed to represent the pre- and post-knee point regions. SoH measurements were fitted to these functions, allowing for accurate prediction of SoH. In commercial cells, the method identified Loss of Lithium Inventory (LLI) as the dominant degradation factor, followed by Loss of Cathode Active Material (LAMC), for more information see Section 2.1.

Data-driven SoH estimation has gained considerable attention due to the increasing availability of online datasets and advancements in machine learning algorithms [13,14]. Compared to mathematical function approaches, these methods offer lower computational complexity by bypassing the development of intricate high-order models. However, the accuracy of data-driven model methods is highly dependent on the quality of the training data and the selected model. Therefore, careful experimental design is essential to ensure the reliability of the data and to determine whether the selected model architecture is appropriate for the given scenario. Additionally, feature engineering, data cleaning, and processing are critical for enhancing estimation accuracy. Moreover, it is essential to incorporate features that are closely correlated with battery degradation.

As previously mentioned, data-driven modeling techniques can be categorized into two distinct approaches. The first approach derives ECM parameters from impedance data, which are then utilized for SoH estimation [15]. In contrast, the second approach directly estimates SoH from impedance measurements, leveraging both real and imaginary part of the impedance at a specific frequency [16].

Considering the first approach, [17] developed a SoH estimation model for second-life batteries using parameters from a first-order ECM, along with an analysis to reduce the number of frequencies examined for improved efficiency. Similarly, [18] compared three different ECMs to fit the EIS data and subsequently developed a Gaussian Process Regression (GPR) model to separately estimate battery cell SoH and SoC from the ECM parameters. Expanding on the use of GPR for SoH estimation, the study in [19] implemented three techniques: one based on all EIS measurements, one using features extracted from model parameters, and one relying on impedance values at specific frequencies.

For the second approach, authors in [20] devised a novel method for SoH estimation using only the frequency, and the real and imaginary part of impedance. Initially, a convolution autoencoder (CAE) is used for feature extraction and the modified data is fed into a Deep Neural Network (DNN) model to estimate the SoH. Similarly, authors in [21] employed a GPR machine learning model for the battery cell SoH estimation using EIS measurements collected in different SoC, SoH and temperature conditions. In [22], authors trained a DNN model for SoH estimation for two different temperatures, and applied a transfer learning technique for estimating the SoH for another temperature, which demonstrated great performance and robustness.

These studies collectively highlight the growing complexity of SoH estimation techniques. While integrating ECMs, Machine Learning (ML) models, and frequency-specific analysis can significantly enhance accuracy, such approaches also introduce challenges, particularly in terms of computational costs and model complexity, which may hinder their practical deployment.

To address these challenges, the innovations presented in this paper aim to improve the performance and usability of SoH estimation methods, utilizing state-of-the-art (SOTA) deep learning models, while exploring new approaches for their practical application. In this paper, the authors developed two methods, Method A and Method B, which use SOTA models for SoH estimation based on ECM and raw EIS data, respectively. Subsequently, the methods and their respective models were compared to evaluate their performance. Following this, they were converted into TinyML models for deployment on micro-controllers. Specifically, the key innovations of this paper are to:

- A comparative analysis of two data-driven modeling approaches for SoH estimation is conducted-one utilizing parameters derived from an ECM, and the other based directly on raw EIS data
- Development of SOTA deep learning models, based on CNN, LSTM and GRU neural networks, for SoH estimation, using EIS data
- Provide guidance for ECM parameters extraction and for the proper training and testing of deep learning models

- Investigate models' performance on various sets of input features, considering also the SoC variations influence at a constant temperature of 25 °C
- Compress and convert the top-performing models into TinyML format, using .tflite libraries, and analyze the effects on model size, latency and performance.

This paper is organized as follows: Section 2 provides an overview of the diagnostics and modeling in battery health assessment, focusing on degradation mechanisms of lithium batteries, EIS and ECMs. Section 3 describes the proposed methodology and the materials used in this work. In particular, the EIS dataset used in the study, the ECM parameter extraction process, the ML model developed for SoH estimation and analyzed and the metrics used for the final results. Section 4 presents the results and discussions, where the performances of the proposed models are compared and analyzed, and the TinyML conversion process is assessed. Finally, Section 5 concludes the paper, summarizing the main findings and proposing future directions for research.

2. Advanced diagnostics and modeling in battery health assessment

Accurate estimation of the SoH of lithium-ion batteries is essential for optimizing performance, ensuring safety, and extending their operational lifespan, particularly in high-demand applications. Once a battery's SoH declines to approximately 80% [23], it becomes unsuitable for use in electric vehicles due to increased thermal and electrical instability under certain environmental conditions. At this point, these batteries are repurposed as 'second-life' batteries [24], finding new applications in less demanding, low-stress environments such as stationary energy storage. Advanced diagnostic techniques and modeling approaches are vital for understanding the complex electrochemical and mechanical degradation mechanisms that influence battery performance and reliability over time. This section delves into key degradation processes and diagnostic methods, with a particular focus on EIS and the development of ECMs to simulate critical internal electrochemical behaviors. By integrating these diagnostics and models, researchers can more accurately predict battery health, optimize operational conditions, and mitigate degradation, ultimately enhancing battery longevity and performance.

2.1. Degradation mechanisms

As Li-ion batteries undergo multiple charge and discharge cycles, various internal electrochemical and mechanical degradation processes begin to occur, including SEI formation, binder decomposition, lithium plating, and particle cracking. These procedures can lead to degradation mechanisms that can be classified to LAM, LLI, Resistance Increment (RI), and Electrolyte Loss (EL) which leads to capacity and power fade (CF and PF) [25].

LAM involves the reduction of electrochemically active material in the electrodes, often caused by mechanical stress, particle cracking, binder decomposition or side reactions, leading to decreased capacity [26]. LLI refers to the irreversible loss of lithium ions, commonly due to the formation and growth of the SEI on the anode or lithium plating, which diminishes the battery's capacity over time. To accurately estimate LAM and LLI, the Incremental Capacity (IC) [dQ/dV] curve and the Differential Voltage (DV) [dV/dQ] curve should be formed [27]. These curves provide valuable insights, by identifying peak and valley values, as well as tracking the shifts in their positions as the battery degrades [28].

RI denotes the increase in internal resistance within the battery, impeding the flow of ions and electrons, and is influenced by factors such as SEI thickening, electrode degradation, and electrolyte decomposition, leading to reduced power output and capacity fade [29,30]. EL pertains to the reduction or degradation of the electrolyte, affecting ion transport, and can result from decomposition due to high voltage or temperature, evaporation, leakage, or side reactions consuming electrolyte components. Initially, EL can present minimal impact, but as the electrolyte becomes severely depleted – particularly towards the end of the battery's lifespan – can result in significant capacity loss [31,32]. Understanding these degradation mechanisms is essential for developing strategies to enhance battery durability and performance.

The rate of capacity and power fade begins to accelerate noticeably near a critical threshold of the battery cell, typically around 70%–80% of SoH, known as the "knee-point". This point is crucial to predict and identify, as the battery's behavior becomes increasingly unpredictable beyond it [33].

As mentioned above SEI layer and lithium plating formation are two key processes affecting the aging and performance of lithium-ion batteries. The SEI layer is formed on the electrode surface during the initial charge process and acts as a protective barrier to inhibit additional interactions between the electrode and electrolyte. Nonetheless, its porous characteristics facilitate electrolyte transfer, resulting in continuous SEI thickening and depletion of active lithium. On the other hand, lithium plating occurs when lithium deposits on the anode surface rather than intercalating into graphite, particularly under situations such as high charge rates, low temperatures, or extended cycling. Plated lithium may react with the electrolyte, resulting in the formation of extra SEI or becoming electrically separated, which causes rapid capacity degradation. In severe cases, lithium dendrites may also formed, which might cause internal short circuits and safety issues [34].

The primary managing factors that contribute to these degradation processes are temperature, C-rate of the charging and discharging profile, Depth of Discharge (DoD), storage time and applied pressure [35]. By carefully adjusting these parameters, researchers can mitigate (or accelerate) battery degradation in a controlled manner, without causing any immediate damage [36].

Overall, to acquire valuable and accurate measurements from the aforementioned degradation mechanisms, expensive laboratory equipment with controllable environmental conditions is required. Moreover, in order to obtain useful data, extensive data processing is required, especially for the IC and DV curves (Savitzky-Golay filter) [37]. For these reasons, EIS technique is preferred for studying the degradation of the battery cell.

2.2. Electrochemical impedance spectroscopy

Electrochemical impedance spectroscopy is a technique used to analyze the electrical properties of materials and their electrochemical behavior across a wide range of frequencies by measuring their impedance. In battery applications, EIS can provide valuable insights into various processes, including ohmic/inductive behavior, SEI and CEI (Cathode-Electrolyte Interphase) formation, lithium plating, diffusion phenomena, structural degradation, and electrolyte decomposition. By adjusting the parameters of an ECM, these processes can be accurately emulated, offering a detailed understanding of the battery's performance, degradation mechanisms, and overall health [38].

Battery cell impedance can be measured using various techniques, depending on the type of excitation signal, such as galvanostatic (current-based) or potentiostatic (voltage-based), and its form, which may be step, sinusoidal, or multi-sine. Additionally, measurements are influenced by the operational state of the battery, either 'in-situ' (during relaxation) or 'in-operando' (during charging or discharging process) modes. Most researchers employ a sinusoidal excitation signal with a small amplitude (current or voltage) when conducting EIS, applying one frequency at a time while the battery is in its 'in-situ' state. Small-amplitude excitation signals are used to ensure that the system remains linear and does not perturb the battery's behavior, enabling a more accurate and reliable measurement of its intrinsic electrochemical properties. It should be emphasized, however, that the

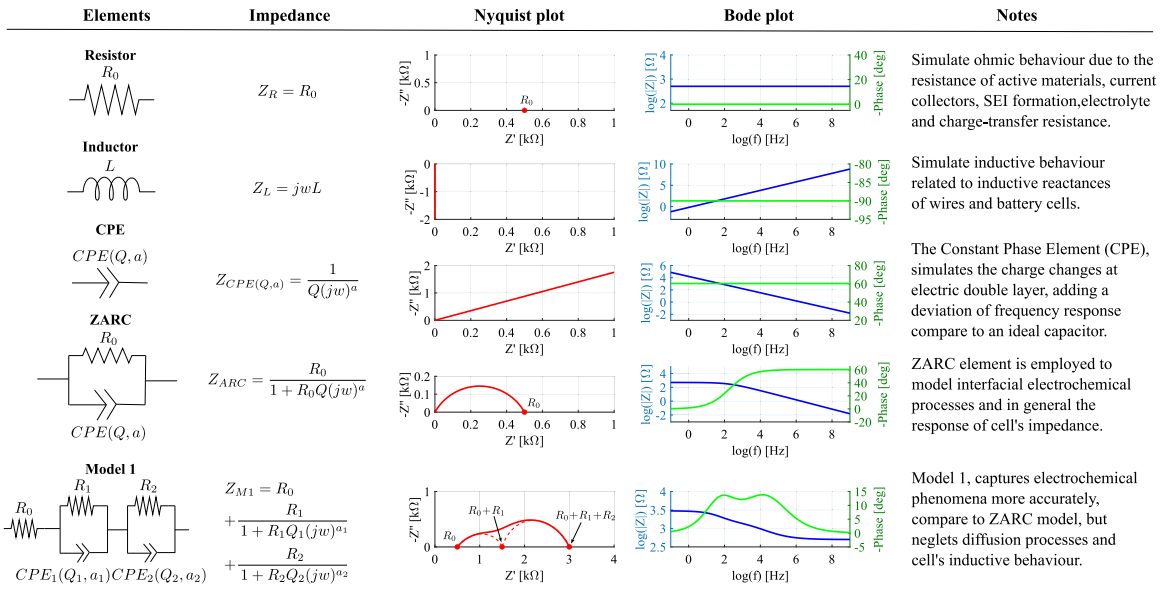

Fig. 1. Different electrical elements (resistor, inductor, Constant Phase Element (CPE), ZARC, and a more complex model) along with their impedance equations, Nyquist plots, Bode plots, and corresponding notes explaining their physical interpretations.

amplitude must not be too small, as this would increase the impact of noise on the measurements. Therefore, a sweet spot must be found to balance linearity and signal quality. By analyzing the corresponding response (voltage or current with respect to the excitation signal), researchers can calculate the total impedance, which consists of both real and imaginary components. [38]. The real part represents the ohmic behavior, while the imaginary part provides insights into the capacitive and inductive behavior of the battery.

To ensure the accuracy of EIS measurements, several criteria must be met, including system linearity, causality, stability, and model fitness [39]. Data quality can be validated by examining the shape of Lissajous plots and using Kramers–Kronig relations [40], both of which serve as robust indicators.

In some BMS applications, performing 'in-situ' EIS measurements is not feasible, primarily due to time constraints. As a result, alternative techniques have been developed to capture EIS data while the battery is 'in-operando' mode [41–43]. However, these methods are complex and often introduce noise due to various interferences. Additionally, it is important to note that impedance measurements are highly sensitive to environmental factors such as temperature, SoC, pressure, and the battery's degradation stage. These variables further complicate the process when EIS tests are conducted in-operando mode.

2.3. Equivalent circuit models

Several models are used to analyze and predict battery behavior, with different trade-offs between accuracy and complexity. The most common are ECMs, single-particle models (SPMs) and pseudo two-dimensional models (P2Ds) [44]. ECMs simulate battery behavior using electrical components, offering a good balance between accuracy and computational efficiency, making them ideal for real-time applications in BMS. However, it is important to note that ECM components do not often represent the true physical characteristics of the battery cell; rather, they are used to emulate its response to different environmental conditions.

SPMs simplify lithium-ion battery modeling by considering ion diffusion within one representative particle per electrode, reducing computational complexity. Conversely, P2D models solve detailed electrochemical equations across electrode thickness and electrolyte regions, capturing spatial gradients accurately, but their complexity limits real-time applicability. ECM models are the most widely used due to their low computational complexity, ease of parametrization and satisfactory accuracy for battery states estimation [45]. These models aim to accurately simulate the internal characteristics and electrochemical processes of the battery cells, including ohmic and inductive resistance, charge-transfer resistance, polarization resistance, double-layer capacitance, and diffusion impedance [18,46]. Although they lack the detailed physical knowledge compare to SPM and P2D models, their simplicity makes them ideal for embedded applications requiring real-time estimation.

Several circuit elements and configurations can be employed to model the internal behavior of battery cells. A typical ECM often incorporates a combination of resistors, inductors, capacitors, Constant Phase Elements (CPEs), and Warburg impedance. Fig. 1 presents an overview of some of the most commonly used electrical components and models, including their general equations, frequency response characteristics with Nyquist and Bode plots and some notes explaining their physical interpretations.

Several tests can be conducted to gather the necessary data for developing an ECM. The most commonly used tests include the Galvanostatic Intermittent Titration Technique (GITT) [47], Hybrid Power Pulse Characterization (HPPC) [48], and EIS [17]. GITT and HPPC provide valuable insights into kinetic parameters, diffusion coefficients, and the SoC-voltage relationship. However, these tests are time-consuming due to long resting periods, and HPPC, in particular, can stress batteries more due to high current pulses. In contrast, EIS, with a proper frequency adjustment, can capture nearly all the internal electrochemical processes of the battery cell without the need for extended resting periods [49].

3. Materials and methods

The proposed methodology follows a structured approach starting with data acquisition and pre-processing, followed by model development, implementation and validation. In this section, a first general overview of the EIS dataset used as model's input is described and the parameter extraction process for the ECM is explained. Next, the performance of the developed data-driven models for SoH estimation were compared by utilizing specific evaluation metrics.

A general overview of the structure of the proposed methodology is shown in Fig. 2 where the two different methods are described. The architecture of Method A, used for SoH estimation, is based on fitting

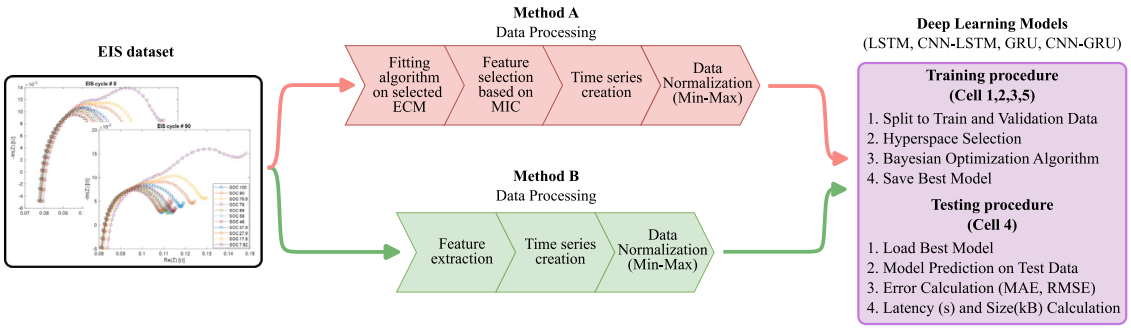

Fig. 2. Architecture of the two developed methods for processing the EIS dataset and training deep learning models. Method A involves ECM fitting, MIC-based feature selection, time series creation, and normalization. Method B uses direct feature extraction followed by time series creation and normalization. Both methods feed deep learning models with a defined training and testing procedure.

ECM parameters to EIS data. For this, the ECM of Fig. 3 was chosen for its ability to emulate various internal electrochemical processes, ensuring high accuracy. The IGWO algorithm was then employed to fit the EIS data, extract the ECM parameter values, and validate their accuracy. In this context, we examined if the ECM parameters fall within an acceptable range and reconstructing the Nyquist plot to ensure it closely matches the original from the EIS dataset. By following this procedure, it is unnecessary to verify the original EIS datasets using the Kramers–Kronig relations, as suggested by some researchers [39, 50]. Afterwards, an input analysis was performed by evaluating the model's performance across various input feature combinations, taking into account the correlation analysis conducted using the Maximum Information Coefficients (MIC) method. The results of this analysis are presented and discussed in greater detail in the following sections. The selected inputs were then converted as time-series data and normalized using min–max normalization to prepare them, with the appropriate format, for models' training and testing.

A similar procedure was also applied to Method B, where the key difference is that ECM development is not required, and feature extraction focuses on obtaining the real and imaginary parts of the measured impedance at a specific frequency.

The models' training and testing procedures that were followed for both methods are the same. Data from Cells 1, 2, 3, and 5 were used to train the models, while data from Cell 4 were reserved exclusively for testing. This approach ensures the models' robustness when applied to unseen datasets. The training data were further divided into training and validation sets with 80% and 20% split, respectively, to prevent overfitting. The authors developed four distinct models, LSTM, CNN-LSTM, GRU, and CNN-GRU, and identified the optimal hyperparameters for each, including the number of units, layers, and activation functions. This was achieved by exploring a defined hyperparameter space, using the Bayesian optimization algorithm, which is discussed in detail in the following sections. Finally, the best-performing models that was identified through the Bayesian optimization algorithm, for each type of neural network, were tested and their performance, evaluated in terms of accuracy, model size, and latency, was thoroughly assessed.

3.1. EIS dataset

The dataset used in this study were analyzed in [51] and it is available online [52]. The battery dataset includes multiple EIS measurements from five 1.1 Ah Li-Po battery cells, measured under varying SoC and SoH conditions. The EIS measurements were taken over a frequency range from 0.2 Hz to 5000 Hz, using an excitation current signal with an amplitude of 40 mA. An example of EIS dataset (Nyquist plots), can be seen in Fig. 2. Additionally, the dataset provides parameters for an ECM, which were obtained through Matlab by applying the *lsqnonlin* function [53] with a multi-start algorithm to avoid convergence to suboptimal local minima: however, in our proposed methodology, the pre-fitted data provided by the dataset [52] will not be used. Although the dataset includes information on battery SoC, it is not suitable for developing a SoC estimation model. This is because the dataset lacks sufficient variation in SoC values with corresponding measurements, which would result in a model that is neither accurate nor robust. For this reason, the authors in this paper, did not attempt to develop such model. Instead, they utilized the provided (true) SoC values to analyze performance response, of the SoH estimation models, when SoC is used as an input.

3.2. Parameter extraction

In this section, authors provide few guidelines of the steps that need to be followed for extracting the parameters of an ECM.

The first step is to select the appropriate ECM. In general, high-precision models have an increased computational cost and complexity, while simpler models offer lower performance but can be implemented more easily. Depending on the application and project requirements, a trade-off between accuracy and complexity must be found. However, to correctly represent the dynamics of the processes taking place within lithium batteries, a model of at least second or third order is typically used [54]. For this reason, the ECM presented in Fig. 3, and also used in [55], was utilized in this work, as it is able to achieve a high accuracy and to optimally represent the dynamics described by the EIS dataset used both for high and low frequencies.

For the second step, an approximation of the initial values of the parameters along with their upper and lower bounds for the selected ECM should be provided. Following this step is essential to ensure that the fitting algorithm identifies the global minimum, rather than a local minimum, resulting in a more accurate estimation of the ECM parameters. This approximation should consider the shape of the Nyquist plot derived from EIS measurements. By analyzing the curve shapes and recognizing electrochemical processes occurring at specific frequencies, it is possible to develop equations that provide an initial approximation of the ECM parameters, while the lower and upper bounds are set based on experience and literature. These approximations can then be used as initial conditions for the fitting algorithm. Authors in [18] provide an analytical guide detailing the procedure that should be followed for extracting those initial parameters. As depicted in Fig. 1 and discussed in Section 2.3, the values of the resistor and inductor can be estimated by analyzing high-frequency data. Similarly, the parameters for the ZARC elements can be determined at medium frequencies. Various combinations of resistance, capacitance, and depression factors can create complex shapes that are capable of fitting most EIS data. Lastly, the Warburg element, which describes the diffusion phenomena, is calculated in the low-frequency domain.

In the final step, selecting a solver to find the global minimum of the objective function, developed based on the selected ECM, is crucial. Accurate approximation of initial values and bounds is essential to ensure that the objective function reaches the global minimum.

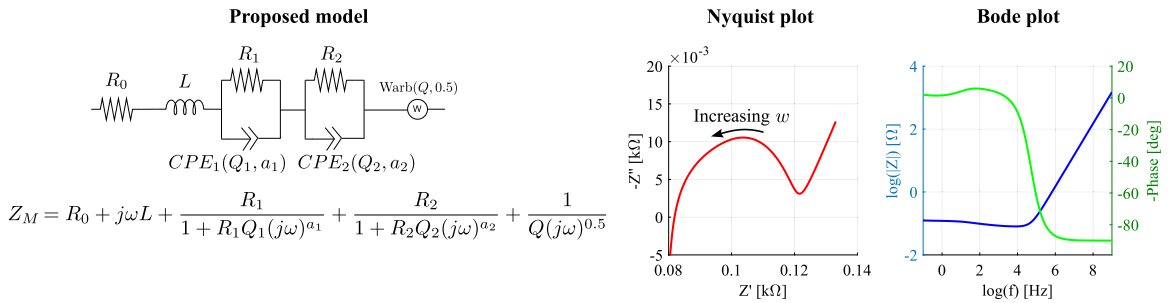

Fig. 3. Characteristics and total impedance equation of the proposed Equivalent Circuit Model, which includes resistive, inductive, constant-phase, and Warburg elements. The corresponding Nyquist and Bode plots illustrate the model's impedance behavior across frequencies.

However, for achieving near-optimal values, this step can be avoided, which simplifies and reduces the computational cost of the overall process. Two algorithms have been analyzed to fit the ECM parameters to the EIS data. The first fitting algorithm follows a similar approach used in [51], utilizing the *lsqnonlin* function with a multi-start algorithm, while the second algorithm is based on the Improved Grey Wolf optimizer (IGWO), a nature-inspired metaheuristic algorithm based on the hierarchical leadership dynamics and collective hunting strategies of wild grey wolves [56]. Both algorithms were implemented in Matlab to extract the parameters of the proposed ECM model from the EIS data. The IGWO solver demonstrated better performance in achieving near-optimal results, when all initial values were set to zero

3.3. Developed models

3.3.1. Neural network architectures

LSTM networks are a subtype of RNNs (which are specifically designed for sequential data processing) developed to improve the RNNs flaws, especially in managing long-term dependencies. An LSTM unit features three gates: input, forget, and output. These gates determine the information to be transmitted to the output, retained in memory, or discarded. This design helps LSTMs maintain information over extended durations, proving essential for handling intricate, sequential tasks like language processing and time series forecasting. LSTMs excel at capturing long-term dependencies and accommodating data sequences of varying lengths, providing a notable edge over basic neural network models [57].

GRUs, akin to LSTMs, are a variant of RNN with a less complex structure. GRUs streamline the process by combining the input and forget gates into one update gate and integrating the cell and hidden states. This simplification makes GRUs easier to train than LSTMs, often yielding similar or better results on specific tasks. The primary distinctions between GRUs and LSTMs revolve around their architectural simplicity and training speed; GRUs are quicker to train but easier to deploy in edge devices. Both GRUs and LSTMs offer advantages over traditional RNNs by mitigating the vanishing gradient issue, thus enhancing the learning of long-distance dependencies in data [58].

Convolutional Neural Networks (CNNs) are highly effective at feature extraction, a fundamental aspect of many machine learning applications. They utilize convolutional layers with learnable filters to detect specific patterns, generating feature maps that highlight important details. Pooling layers then refine these maps by reducing their spatial dimensions through techniques like max pooling, which selects the highest value, or average pooling, which computes the mean. This process not only decreases computational cost and memory usage but also improves the model's ability to generalize, making CNNs well-suited for a wide range of visual recognition tasks [59].

In this paper, authors developed four different models (LSTM, CNN-LSTN, GRU and CNN-GRU) for the SoH estimation, as they constitute the 'state-of-the-art' models specific for time-series estimations. The CNN-LSTM and CNN-GRU fused model combines convolutional layers for feature extraction with LSTM layers for capturing temporal dependencies. CNN layers detect spatial patterns, while LSTM layers handle sequence learning, making the model effective for time-series data with complex features.

3.3.2. Bayesian hyperparameter optimization

A major challenge in data-driven approaches is the optimization of hyperparameters, which play a critical role in determining model performance. Selecting the right combination of parameters, such as learning rate, batch size, number of layers, and activation functions, can significantly impact convergence speed, generalization ability, and overall accuracy. Poorly chosen hyperparameters may lead to issues like overfitting, underfitting, or slow training times. To determine the optimal set of hyperparameters, various methods such as Grid Search (GS), Manual Search (MS), and Random Search (RS) can be employed. However, GS and MS tend to be computationally intensive, particularly when dealing with a high number of hyperparameters or an extensive search space. Moreover, RS operates as a purely stochastic technique, which may lead to inefficient exploration of the parameter space in the search for optimal values. In contrast, probabilistic methods like Bayesian optimization offer an effective alternative by integrating the strengths of these traditional techniques and achieving near-optimal results with fewer evaluations, as they utilize information from prior evaluations [60].

Bayesian Hyperparameter Optimization (BHO) is an iterative method specifically designed to efficiently locate the global optimum of complex functions. It employs a probabilistic surrogate model, commonly a Gaussian process, to approximate the target function's behavior and associated uncertainty. This surrogate model facilitates the optimization process by balancing exploration (investigating uncharted areas of the hyperparameter space) and exploitation (focusing on regions predicted to yield better results). At each iteration, BHO determines the next set of parameters to evaluate using an acquisition function that measures this balance. Once the selected parameters are evaluated, the surrogate model is updated, and the process is repeated until convergence is achieved or a predefined stopping criterion is met [61].

In this paper, BHO was utilized in order to find the optimal set of parameters that achieves the best accuracy. The hyperspace's parameters were carefully selected in order to be compatible with .tflite libraries for compressing this models for the next step. BHO algorithm searched through several type of parameters such as the number of layers, units, filters, learning rate and activation functions of LSTM, GRU and CNN layers to find the optimal combination.

3.4. Metrics

For evaluating the model's performance in terms of accuracy, the Mean Absolute Error (MAE) and Root Mean Squared Error (RMSE) are used, calculated as in Eqs. (1) and (2), respectively:

$$RMSE = \sqrt{\frac{1}{n}\sum_{i=1}^{n}(y - \hat{y})^2} \tag{1}$$

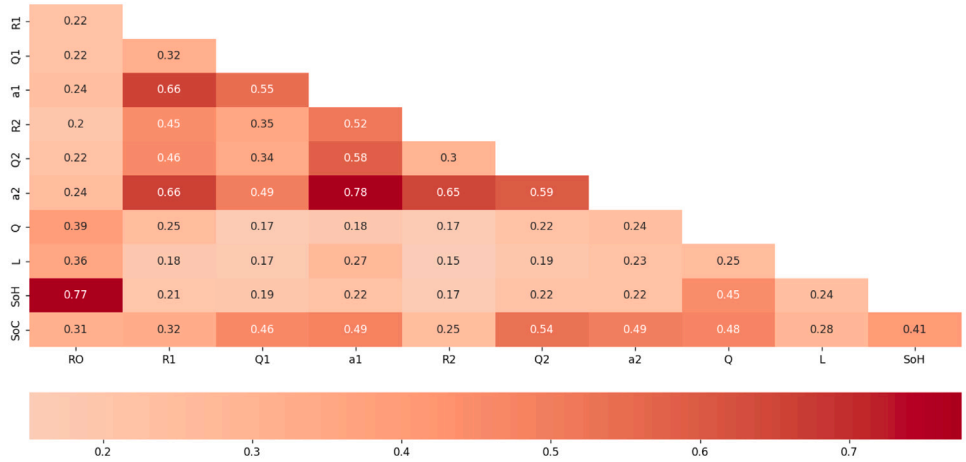

Fig. 4. Maximum Information Coefficients between ECM parameters and battery SoH and SoC, which highlight the relative strength of non-linear associations. Higher MIC values indicate stronger dependencies, helpful for feature selection.

Table 1
Performance metrics (MAE, RMSE, and model size) for Method A using different input feature combinations across LSTM, CNN-LSTM, GRU, and CNN-GRU models. The table shows the impact of various ECM parameters and state indicators (SoC, Q) on SoH prediction accuracy: the best result (lowest RMSE) for each model is underlined.

Input features	LSTM			CNN-LSTM			GRU			CNN-GRU		
	MAE (%)	RMSE (%)	Size (kB)	MAE (%)	RMSE (%)	Size (kB)	MAE (%)	RMSE (%)	Size (kB)	MAE (%)	RMSE (%)	Size (kB)
R0	2.41	3.51	1.48	2.16	3.51	3.59	2.17	3.30	3.02	2.26	3.70	2.76
R0, SoC	1.84	3.08	3.98	2.25	3.27	3.59	1.57	3.05	2.99	1.90	3.17	2.78
R0, Q	1.50	**1.80**	1.79	1.43	**1.71**	3.59	1.27	1.62	1.75	1.38	**1.73**	2.77
R0, Q, SoC	1.47	1.84	2.70	1.35	2.36	3.60	1.56	1.80	3.25	1.65	2.64	2.78
R0, R1, Q1, a1, R2, Q2, a2, Q, L	1.54	2.25	1.22	2.07	2.70	3.61	1.15	**1.55**	1.66	2.30	3.04	2.79
R0, R1, Q1, a1, R2, Q2, a2, Q, L, SoC	2.19	2.80	2.40	1.50	1.90	3.62	3.14	3.85	1.64	1.94	2.80	2.80

$$MAE = \frac{1}{n}\sum_{j=1}^{n}|y - \hat{y}| \tag{2}$$

where y is the real value of the SoH and $\hat{y}$ is the predicted value generated by the model. MAE evaluates the average magnitude of prediction errors without considering their direction, offering a clear and straightforward measure of model accuracy. In contrast, RMSE places greater emphasis on larger errors due to its squared error calculation, making it more sensitive to outliers. For the latter, in this paper authors put greater emphasis on RMSE values over MAE. Additionally, the model's size (in kB) and latency (time in seconds for making one prediction) are used as indicators of computational cost, as accurately calculating Floating-Point Arithmetic Operations per second (FLOPs) is not feasible for .tflite models. As a result, FLOPs values cannot be used for direct comparison between .h5 and .tflite models.

4. Results and discussions

4.1. Method A

As it was mentioned above, to investigate the correlation of the ECM parameters with the SoH and SoC, an input analysis based on MIC method were performed. MIC was selected over some other types like, Pearson and Spearman, because it can capture more complex and non-linear relationships among data [62]. As it is shown in Fig. 4, the parameters R0 and Q (Warburg capacitance) provide higher correlation with the SoH, 0.77 and 0.45 respectively, whereas parameters such as Q1,a1,Q2,a2 (ZARC elements) relates more with the SoC. As it was expected, the ZARC elements also provide high correlation with each other, as they form the cycle (or two cycles depending on their values) that appears in the Nyquist plot of EIS data.

It is important to note that SoC values alone are not directly relate with SoH. However, when analyzed with ECM parameters, SoC can offer valuable insight into the battery's degradation stage. This is because ECM parameters reflect the underlying electrochemical processes within the cell, which are highly dependent on SoC. As SoC changes, so do factors such as open-circuit voltage, ion concentration, reaction kinetics, and internal resistive behavior. These shifts influence key ECM parameters, including resistances and capacitances, making SoC an important feature for battery health diagnostics.

In this method, authors assessed the performance of four different models, LSTM, CNN-LSTM, GRU, and CNN-GRU, using six distinct input features, as shown in Table 1. They also investigated the effect of incorporating SoC values alongside ECM parameters to determine if this combination could improve overall model performance. It is important to note that the SoC data used as inputs were not generated by another model but represented actual measured values.

In Table 1, the results of Method A are presented, highlighting the best performance of each model based on the RMSE metric. Additionally, Fig. 5 shows the comparison of the performance of various deep learning models for estimating the SoH using method A over several cycles. Real SoH values are shown together with the predictions made by the LSTM, CNN-LSTM, GRU and CNN-GRU models. The x-axis represents the number of cycles, while the y-axis shows the SoH values. Each model follows the degradation trend over time with different levels of accuracy. In particular, the GRU and CNN-GRU models seem to follow the trajectory of the actual SoH more closely than LSTM and CNN-LSTM, especially in the latter stages of degradation. The figure also shows, with a horizontal arrow, that each cycle interval includes multiple estimates of SoH at different SoC levels, ranging from 100% to 0%.

All the DL models achieved low error, without being computationally expensive, with the GRU model demonstrating the best performance. When all the ECM parameters were used as inputs, the GRU model achieved an RMSE of 1.55% and an MAE of 1.15%. It is worth

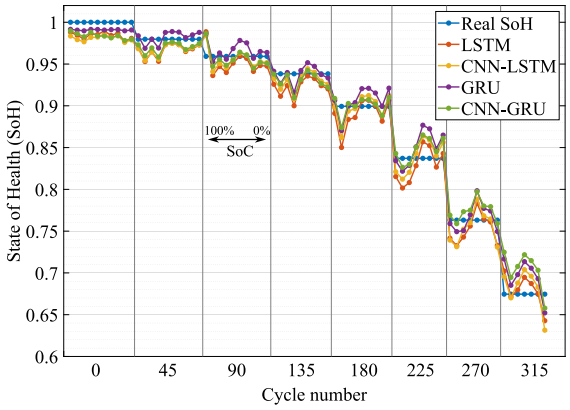

Fig. 5. Performance comparison of the best deep learning models using Method A for SoH estimation across battery cycles. The predictions from LSTM, CNN-LSTM, GRU, and CNN-GRU are evaluated against the real SoH. Each cycle includes multiple data points corresponding to different SoC levels, as indicated by the horizontal arrow.

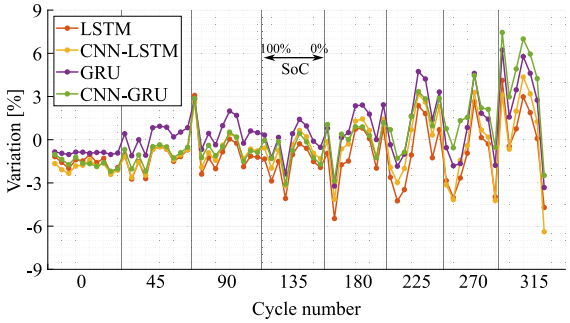

Fig. 6. SoH percentage variation of the best deep learning models using Method A across battery cycles, evaluated against the real SoH. Each cycle includes multiple data points corresponding to different SoC levels, as indicated by the horizontal arrow.

noting that combining models (e.g. CNN with LSTM/GRU) does not always lead to improved accuracy, while the increase in model size is noticeable in most cases. It must be underlined that the size of the models does not depend on the number of input features. Instead, their size, which is determined by the number of learnable parameters, is controlled by the combination of the hyperparameters that the BHO algorithm found. Furthermore, the performance of the models remains nearly unchanged, showing no significant improvement when real SoC values are used as inputs or when all ECM parameters are included. For instance, satisfactory SoH estimation results were achieved across all models by using just the R0 and Q parameters, as shown in Fig. 4. Based on these findings, the complexity of both ECM and DL models can be effectively reduced without compromising accuracy.

Moreover, Fig. 6 depicts the percentage variation of each model with respect the actual SoH values. The figure also shows, with a horizontal arrow, that each cycle interval includes multiple estimates of SoH at different SoC levels, ranging from 100% to 0%. The percentage variation of each model is calculated as in Eq. (3)

$$Var[\%] = \frac{\hat{SoH} - SoH}{SoH} \cdot 100 \tag{3}$$

where SoH is the actual SoH, and $\hat{SoH}$ is the estimated SoH of the considered model.

Considering Fig. 6, it is noticeable that all models demonstrated improved performance during the initial stages of degradation. However, as the battery ages and approaches the 'knee-point', (around 70/% of SoH) the accuracy of the models significantly declines. This pattern is expected since the degradation process of battery cells can be considered a partially stochastic process, due to small variations introduced

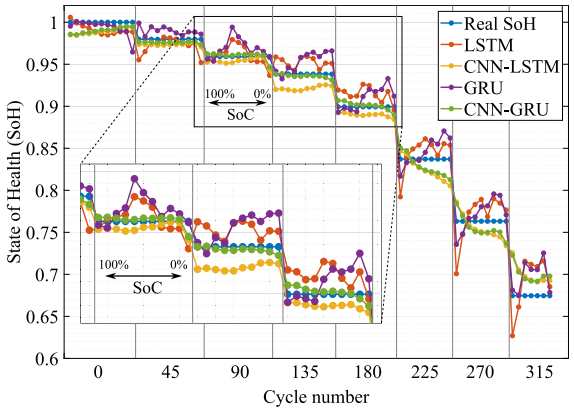

Fig. 7. Performance comparison of the best deep learning models using Method B for SoH estimation across battery cycles. The predictions from LSTM, CNN-LSTM, GRU, and CNN-GRU are evaluated against the real SoH. Each cycle includes multiple data points corresponding to different SoC levels, as indicated by the horizontal arrow.

during the manufacturing process that led to slight differences in their internal resistance. These small differences become more pronounced as the battery moves further into degradation, where variations in SEI layer growth and lithium plating formation are amplified

4.2. Method B

Although models based on the Method A architecture delivered satisfactory results with high accuracy, the overall design and process required for a single SoH estimation are complex and unsuitable for real-time applications. Additionally, due to the sensitivity of EIS data, the values of the ECM parameters can fluctuate even when environmental conditions remain unchanged. This variability can lead to significant errors in real-life applications, where external noise in the measurements is high. To address this, a simplified architecture (referred to as Method B) is proposed. This method estimates the battery cell SoH by directly utilizing raw EIS data as input for a DL model, as illustrated in Fig. 2.

Similar to the previous approach, Method B involved analyzing the same DL models using six different input features derived from combinations of frequency, and the real and imaginary parts of the impedance data from EIS dataset as presented in Table 2. In this method the influence of the SoC as an input parameter were also examined. The main objective was to evaluate the models' accuracy when utilizing just the raw EIS data and compare their performance with the models used in Method A.

Table 2, showcases the results of Method B, emphasizing the best performance achieved by each model based on the RMSE metric. Moreover, Fig. 7 presents a comparison of the performance of advanced deep learning models for estimating SoH using method B. The plot compares the predictions made by the LSTM, CNN-LSTM, GRU and CNN-GRU models with the actual (real) values of SoH. The x-axis represents the number of cycles and the y-axis indicates the SoH. The zoomed area allows a closer look at the estimated SoH, highlighting discrepancies in model predictions at different stages of degradation. The inclusion of multiple data points within each cycle reflects different levels of SoC, as underlined by the horizontal arrows in the insets. Among the models, GRU and CNN-GRU generally maintain closer alignment with the actual SoH, although variations emerge under different SoC conditions.

In this case also, the DL models demonstrated high performance without being computationally expensive, with the CNN-GRU model delivering the best results. When raw EIS input features (frequency, and the real and imaginary parts of impedance) were used, the CNN-GRU model achieved an RMSE of 1.20% and an MAE of 0.87%, as it can be also seen from the zoom area of Fig. 7 with more details. Notably,

Table 2
Performance metrics (MAE, RMSE, and model size) for Method B using different input feature combinations across LSTM, CNN-LSTM, GRU, and CNN-GRU models. Results show how real and imaginary parts of impedance, with or without SoC, influence SoH prediction accuracy: the best result (lowest RMSE) for each model is underlined.

Input features	LSTM			CNN-LSTM			GRU			CNN-GRU		
	MAE (%)	RMSE (%)	Size (kB)	MAE (%)	RMSE (%)	Size (kB)	MAE (%)	RMSE (%)	Size (kB)	MAE (%)	RMSE (%)	Size (kB)
Freq, Z_real	1.77	2.47	1.05	1.31	1.66	2.50	1.31	1.92	0.83	1.40	1.68	2.09
Freq, Z_real, SoC	1.65	2.45	2.71	1.47	1.76	2.51	1.89	2.59	1.61	1.76	2.14	2.10
Freq, Z_im	2.73	3.28	3.06	3.66	4.43	2.15	2.67	3.30	1.85	3.87	4.73	1.74
Freq, Z_im, SoC	1.53	**1.92**	2.24	4.10	5.10	1.52	1.36	**1.77**	3.42	3.91	4.80	1.56
Freq, Z_real, Z_im	1.67	2.67	1.06	1.25	**1.48**	2.51	1.84	2.72	2.91	0.87	**1.20**	2.18
Freq, Z_real, Z_im, SoC	2.27	3.35	3.2	1.84	2.44	2.51	1.94	3.03	1.53	1.52	2.02	1.26

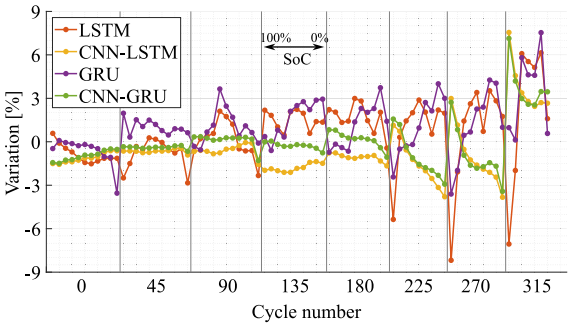

Fig. 8. SoH percentage variation of the best deep learning models using Method B across battery cycles, evaluated against the real SoH. Each cycle includes multiple data points corresponding to different SoC levels, as indicated by the horizontal arrow.

Table 3
Percentage reduction in latency and model size after converting to TensorFlow Lite (.tflite) format for the models using different input features. All models show significant reductions, making them suitable for deployment on resource-constrained devices.

Models	Reduction	Input features		
	(%)	Freq, Z_real	Freq, Z_im	Freq, Z_real, Z_im
LSTM	Latency	99.53	99.35	99.35
	Size	89.97	90.84	89.91
CNN-LSTM	Latency	99.92	99.92	99.71
	Size	87.66	89.78	87.65
GRU	Latency	99.48	99.33	99.01
	Size	89.24	89.50	90.87
CNN-GRU	Latency	99.90	99.93	99.87
	Size	86.66	88.80	89.77

both the CNN-LSTM and CNN-GRU models exhibited very low errors when these input features were utilized, without any size increasement compare with LSTM and GRU models. Similarly, by using only the frequency, the imaginary part, and the SoC as inputs, the LSTM and GRU models achieved high accuracy, with errors below 2% in both cases. It is important to note that while the true SoC input cannot be used in real-time applications (only the estimated values of SoC), this study aimed to examine its influence on model performance, which was found to be negligible.

In addition, Fig. 8 depicts the percentage variation of each model with respect the actual SoH values, calculated as in Eq. (3). The figure also shows, with a horizontal arrow, that each cycle interval includes multiple estimates of SoH at different SoC levels, ranging from 100% to 0%. Similarly with Method A, models achieved better results in early stages, and when the degradation stage moved near to the 'knee-point', the performance degrades since the battery behavior become more 'unpredictable'.

Comparing these methods reveals that Method B not only achieves higher accuracy but also simplifies the SoH estimation process. Unlike other approaches, it eliminates the need to develop an ECM, fit data, or extract parameters. With just basic data processing steps, such as time-series creation and data normalization, Method B can deliver highly accurate SoH estimations. Furthermore, the model sizes are within an acceptable range for deployment on most hardware devices, but their reduction is necessary for optimal performance. However, to further reduce computational cost, model size, and latency, converting these models into TinyML implementations is necessary, as discussed in the next section.

4.3. TinyML conversion

Data-driven models offer a simple yet highly accurate solution for various BMS tasks, making their efficient deployment on edge devices an increasingly relevant topic, commonly referred to as TinyML. Embedded sensor devices can continuously feed real-time data to TinyML models for estimating SoC [63], SoH [64], and RuL [65]. However, deploying these models on low-power and low-resources devices requires significant compression to minimize energy consumption and memory while maintaining accuracy.

There are plenty of quantization methods (Quantization [66], Weight pruning [67], transfer learning [68]) and software that can be utilized to compress and convert deep learning models into TinyML. In this case, authors exported the TensorFlow models into .h5 format and, afterwards, used `TFLITE` libraries [69] to quantize the models from 32 bit floating-point numbers (float32) to 8 bit integers (int8). Specifically, for each model, a `TFLiteConverter` instance was created from the corresponding saved model directory, and post-training dynamic range quantization was applied by setting `converter.optimizations = [tf.lite.Optimize.DEFAULT]`. This approach reduces model size by converting only the weights from float32 to int8, while keeping activations in float. To ensure compatibility with a broader range of TensorFlow operations – especially those not originally supported by TensorFlow Lite – `allow_custom_ops = True` was enabled, and `converter.target_spec.supported_ops` was set to include both `TFLITE_BUILTINS` and `SELECT_TF_OPS`. This allowed for successful conversion of models that incorporate complex or custom layers without requiring architecture modifications.

Following this procedure, the model's size and its latency (time in seconds for a single prediction), will be decreased significantly as it is presented on Table 3. Afterwards, the generated model should be converted into an hexadecimal representation, and the proper libraries should be included into the device, in order to be able to perform real-time estimations on a micro-controller. The models can be transformed into C code using tools such as the xxd -i command (Linux command), which converts the .tflite model into a C header file containing the model as a byte array, or utilizing software environments like MATLAB which offer automatic C code generation for trained models, with the added flexibility of targeting specific hardware configurations.

As previously mentioned, TinyML requires simple models and architectures to minimize computational cost. Consequently, models based on Method A and those using SoC as an input feature are excluded, as

extracting this information requires the development of more complex models. Table 3 illustrates the reduction in latency (per batch) and model size (kB) achieved through conversion to the .tflite format.

It is worth noting that the deep learning models were trained using an NVIDIA GeForce RTX 3060 GPU, while the .tflite models were tested, and their latency measured, on a 13th Gen Intel(R) Core(TM) i7-13700F CPU. On average, latency was reduced by 99.61%, while model size presented an 89.22% reduction. The latency of the generated .tflite models ranged from 0.4 ms to 5.85 ms, and their sizes ranged from 90 kB to 310 kB. Additionally, the compatibility and size of libraries (e.g., tflite-micro) should be carefully considered before model development, as not all layers, activation functions, or operations are supported. For example, currently there is no available library from tflite-micro that supports GRU (only for LSTM).

Finally, it is worth noting that the accuracy of the compressed models, those using Freq, Z_real and Freq, Z_real, Z_im, remained practically unchanged, with negligible or no performance degradation. Specifically, the average difference between the quantized and non-quantized models was only 0.05% and 0.042% in terms of MAE and RMSE, respectively, for the first model (Freq, Z_real), and 0.069% and 0.057% for the second model (Freq, Z_real, Z_im). The small differences can be justified by the selected compression technique, which is based on data-type compression rather than layer-wise compression. Unlike layer-wise techniques that modify the network structure and typically require re-training to maintain accuracy, data-type compression mainly affects numerical precision and often preserves model performance without the need for full re-training.

Considering the case of the compressed models that utilized the input features Freq and Z_im, the quantized versions showed an increase in MAE and RMSE errors, that is not acceptable, which can be attributed to the higher numerical sensitivity of Z_im. This feature may introduce greater variance or lower dynamic range, making the model more susceptible to the reduced precision effects introduced by quantization. However, this accuracy degradation can be minimized by re-training the models using a representative subset of the dataset which allows the model to adapt to the reduced precision during the training process. Similarly, performance variations, including small changes in error and model size reduction due to quantization, were also observed in [65], though with different types of models.

5. Conclusion

Accurately estimating a battery's degradation is essential for optimal performance and safety. Among various techniques, EIS is the most effective method, providing direct insights into degradation, while data-driven models excel in leveraging EIS data for precise SoH estimation.

In this paper, two methods (A and B) are proposed using state-of-the-art data-driven models for SoH estimation based on EIS data. Method A depends on the development of an ECM, whereas Method B adopts a much simpler architecture, using only raw EIS data for SoH estimation.

Models based on Method B deliver comparable or, in some cases, superior results to those of Method A. Among these, the CNN-GRU model from Method B achieved the highest accuracy, with an RMSE of 1.20% and an MAE of 0.87%. As clearly demonstrated, the models achieve high accuracy in estimating the SoH during the early stages of battery life. However, their performance significantly deteriorates as the batteries progress further into the degradation stage.

Although the combination of CNN and GRU networks, in some cases, can result in larger model sizes compared to other architectures, this can be significantly reduced by converting the models to the .tflite format with minimal loss of accuracy in most cases. On average, this conversion led to an 89.22% reduction in model size and a 99.61% decrease in latency. These .tflite-converted models can be efficiently deployed on edge devices using appropriate TFLite Micro libraries, enabling real-time SoH estimation.

Considering the future research, smaller, simpler and more accurate DL models should be developed in order to be converted into TinyML models. Furthermore, it is necessary the development of hardware devices that can perform EIS measurements supporting DL models, with optimize operation, for real-time SoH estimations. Additionally, all the aforementioned data and analysis is based on specific measurements that were conducted in 5 battery cells, with certain type, under 'in-situ' mode. To enhance the accuracy and robustness, of the developed models, a more spherical battery dataset is needed, that will provide EIS data for several and different battery types, dynamic conditions ('in-operando') and different stress conditions, such as C-rates, temperatures and pressures. Lastly, in order to reduce the time of EIS experiments, an accurate mapping of electrochemical processes with certain frequencies and impedance values need to be developed for the most commonly used types such as NMC and LFP cells.

CRediT authorship contribution statement

Spyridon Giazitzis: Writing – original draft, Visualization, Validation, Software, Methodology, Investigation, Formal analysis, Conceptualization. **Abdisamad Ahmed Isse:** Software, Data curation. **Nicola Blasuttigh:** Writing – review & editing, Visualization, Validation, Supervision. **Alessandro Massi Pavan:** Writing – review & editing, Validation. **Davide M. Raimondo:** Writing – review & editing, Validation. **Susheel Badha:** Writing – review & editing, Validation. **Filippo Rosetti:** Writing – review & editing, Validation. **Emanuele Ogliari:** Writing – review & editing, Validation, Supervision, Methodology, Conceptualization.

Declaration of competing interest

The authors declare that they have no known competing financial interests or personal relationships that could have appeared to influence the work reported in this paper.

Data availability

Data are available online.

References

[1] Nikolas G Chatzigeorgiou, Spyros Theocharides, George Makrides, George E Georghiou, A review on battery energy storage systems: Applications, developments, and research trends of hybrid installations in the end-user sector, J. Energy Storage 86 (2024) 111192.

[2] Konstantinos Oureilidis, Kyriaki-Nefeli Malamaki, Konstantinos Gallos, Achilleas Tsitsimelis, Christos Dikaiakos, Spyros Gkavanoudis, Milos Cvetkovic, Juan Manuel Mauricio, Jose Maria Maza Ortega, Jose Luis Martinez Ramos, et al., Ancillary services market design in distribution networks: Review and identification of barriers, Energies 13 (4) (2020) 917.

[3] Dapai Shi, Jingyuan Zhao, Chika Eze, Zhenghong Wang, Junbin Wang, Yubo Lian, Andrew F Burke, Cloud-based artificial intelligence framework for battery management system, Energies 16 (11) (2023) 4403.

[4] Yuanyuan Pan, Ke Xu, Ruiqiang Wang, Honghong Wang, Guodong Chen, Kai Wang, Lithium-ion battery condition monitoring: A frontier in acoustic sensing technology, Energies 18 (5) (2025) 1068.

[5] Yiwen Sun, Hengwei Xie, Qi Diao, Hongzhang Xu, Xiaojun Tan, Yuqian Fan, Liangliang Wei, A novel SOH estimation method with attentional feature fusion considering differential temperature features for lithium-ion batteries, IEEE Trans. Instrum. Meas. (2024).

[6] Jaekwang Kim, Byambasuren Gerelt-Od, Eunseon Shin, Hyunchul Kang, Nayeong Kim, Changshin Jo, Hyungbin Son, Songhun Yoon, State of health monitoring by gas generation patterns in commercial 18,650 lithium-ion batteries, J. Electroanal. Chem. 907 (2022) 115892.

[7] Shujuan Hou, Yue Fan, Bowen Dou, Hai Li, Qin Zhang, Hao-sen Chen, Strain feature-assisted state of health estimation for lithium-ion batteries, Energy (2025) 136058.

[8] Ximena Carolina Acaro Chacón, Stefano Laureti, Marco Ricci, Gregorio Cappuccino, A review of non-destructive techniques for lithium-ion battery performance analysis, World Electr. Veh. J. 14 (11) (2023) 305.
[9] Laurence A Middlemiss, Anthony JR Rennie, Ruth Sayers, Anthony R West, Characterisation of batteries by electrochemical impedance spectroscopy, Energy Rep. 6 (2020) 232–241.
[10] Zheyuan Pang, Kun Yang, Zhengxiang Song, Pengcheng Niu, Guangyang Chen, Jinhao Meng, A new method for determining SOH of lithium batteries using the real-part ratio of EIS specific frequency impedance, J. Energy Storage 72 (2023) 108693.
[11] Qunming Zhang, Cheng-Geng Huang, He Li, Guodong Feng, Weiwen Peng, Electrochemical impedance spectroscopy based state-of-health estimation for lithium-ion battery considering temperature and state-of-charge effect, IEEE Trans. Transp. Electr. 8 (4) (2022) 4633–4645.
[12] Pietro Iurilli, Claudio Brivio, Rafael E Carrillo, Vanessa Wood, Physics-based SoH estimation for li-ion cells, Batteries 8 (11) (2022) 204.
[13] Eunsong Kim, Minseon Kim, Juo Kim, Joonchul Kim, Jung-Hwan Park, Kyoung-Tak Kim, Joung-Hu Park, Taesic Kim, Kyoungmin Min, Data-driven methods for predicting the state of health, state of charge, and remaining useful life of li-ion batteries: A comprehensive review, Int. J. Precis. Eng. Manuf. 24 (7) (2023) 1281–1304.
[14] Seyed Mahdi Miraftabzadeh, Andrea Di Martino, Michela Longo, Dario Zaninelli, Deep learning in power systems: A bibliometric analysis and future trends, IEEE Access (2024).
[15] Yanshuo Liu, Licheng Wang, Dezhi Li, Kai Wang, State-of-health estimation of lithium-ion batteries based on electrochemical impedance spectroscopy: a review, Prot. Control. Mod. Power Syst. 8 (3) (2023) 1–17.
[16] Jian Wu, Jinhao Meng, Mingqiang Lin, Wei Wang, Ji Wu, Daniel-Ioan Stroe, Lithium-ion battery state of health estimation using a hybrid model with electrochemical impedance spectroscopy, Reliab. Eng. Syst. Saf. 252 (2024) 110450.
[17] Marcelo Miranda Camboim, Aghatta Cioquetta Moreira, NC Maria de Fátima, Raul Fernando Beck, Vitor Torquato Arioli, Camila Omae, Hongwu Ding, State of health estimation of second-life batteries through electrochemical impedance spectroscopy and dimensionality reduction, J. Energy Storage 78 (2024) 110063.
[18] Francesco Santoni, Alessio De Angelis, Antonio Moschitta, Paolo Carbone, Matteo Galeotti, Lucio Cinà, Corrado Giammanco, Aldo Di Carlo, A guide to equivalent circuit fitting for impedance analysis and battery state estimation, J. Energy Storage 82 (2024) 110389.
[19] Bo Jiang, Jiangong Zhu, Xueyuan Wang, Xuezhe Wei, Wenlong Shang, Haifeng Dai, A comparative study of different features extracted from electrochemical impedance spectroscopy in state of health estimation for lithium-ion batteries, Appl. Energy 322 (2022) 119502.
[20] Josue Obregon, Yu-Ri Han, Chang Won Ho, Devanadane Mouraliraman, Chang Woo Lee, Jae-Yoon Jung, Convolutional autoencoder-based SOH estimation of lithium-ion batteries using electrochemical impedance spectroscopy, J. Energy Storage 60 (2023) 106680.
[21] Yunwei Zhang, Qiaochu Tang, Yao Zhang, Jiabin Wang, Ulrich Stimming, Alpha A Lee, Identifying degradation patterns of lithium ion batteries from impedance spectroscopy using machine learning, Nat. Commun. 11 (1) (2020) 1706.
[22] Yichun Li, Mina Maleki, Shadi Banitaan, State of health estimation of lithium-ion batteries using EIS measurement and transfer learning, J. Energy Storage 73 (2023) 109185.
[23] Lluc Canals Casals, Marta Rodríguez, Cristina Corchero, Rafael E Carrillo, Evaluation of the end-of-life of electric vehicle batteries according to the state-of-health, World Electr. Veh. J. 10 (4) (2019) 63.
[24] Panagiotis Eleftheriadis, Sonia Leva, Manfredi Gangi, Alberto Valdes Rey, Andrea Borgo, Giacomo Coslop, Emanuele Groppo, Lorenzo Grande, Melissa Sedzik, Second life batteries: Current regulatory framework, evaluation methods, and economic assessment: Reuse, refurbish, or recycle, IEEE Ind. Appl. Mag. 30 (1) (2023) 46–58.
[25] M.M. Kabir, Dervis Emre Demirocak, Degradation mechanisms in Li-ion batteries: a state-of-the-art review, Int. J. Energy Res. 41 (14) (2017) 1963–1986.
[26] Francisco J Méndez-Corbacho, David Nieto-Castro, Iñaki Moreno-Artabe, Diego del Olmo, Giorgio Baraldi, Elixabete Ayerbe, DEST: A simplified model and automated tool for loss of lithium inventory and loss of active material estimation in li-ion batteries, ChemElectroChem 11 (5) (2024) e202300830.
[27] Linfeng Zheng, Jianguo Zhu, Dylan Dah-Chuan Lu, Guoxiu Wang, Tingting He, Incremental capacity analysis and differential voltage analysis based state of charge and capacity estimation for lithium-ion batteries, Energy 150 (2018) 759–769.
[28] Gyuwon Seo, Jaeyun Ha, Moonsu Kim, Jihyeon Park, Jaewon Lee, Eunoak Park, Sungyool Bong, Kiyoung Lee, Soon Jong Kwon, Seung-pil Moon, et al., Rapid determination of lithium-ion battery degradation: High C-rate LAM and calculated limiting LLI, J. Energy Chem. 67 (2022) 663–671.
[29] Jun Peng, Xuan Zhao, Jian Ma, Dean Meng, Shuhai Jia, Kai Zhang, Chenyan Gu, Wenhao Ding, State of health estimation of li-ion battery via incremental capacity analysis and internal resistance identification based on Kolmogorov–Arnold networks, Batteries 10 (9) (2024).
[30] Aravinda R Mandli, Anshul Kaushik, Rajkumar S Patil, Arunava Naha, Krishnan S Hariharan, Subramanya M Kolake, Seongho Han, Wooin Choi, Analysis of the effect of resistance increase on the capacity fade of lithium ion batteries, Int. J. Energy Res. 43 (6) (2019) 2044–2056.
[31] E Sarasketa-Zabala, Frederic Aguesse, Igor Villarreal, LM Rodriguez-Martinez, Carmen M López, Pierre Kubiak, Understanding lithium inventory loss and sudden performance fade in cylindrical cells during cycling with deep-discharge steps, J. Phys. Chem. C 119 (2) (2015) 896–906.
[32] Xuebing Han, Languang Lu, Yuejiu Zheng, Xuning Feng, Zhe Li, Jianqiu Li, Minggao Ouyang, A review on the key issues of the lithium ion battery degradation among the whole life cycle, ETransportation 1 (2019) 100005.
[33] Kailong Liu, Xiaopeng Tang, Remus Teodorescu, Furong Gao, Jinhao Meng, Future ageing trajectory prediction for lithium-ion battery considering the knee point effect, IEEE Trans. Energy Convers. 37 (2) (2021) 1282–1291.
[34] Xiao-Guang Yang, Yongjun Leng, Guangsheng Zhang, Shanhai Ge, Chao-Yang Wang, Modeling of lithium plating induced aging of lithium-ion batteries: Transition from linear to nonlinear aging, J. Power Sources 360 (2017) 28–40.
[35] Laxman Timilsina, Payam R Badr, Phuong H Hoang, Gokhan Ozkan, Behnaz Papari, Christopher S Edrington, Battery degradation in electric and hybrid electric vehicles: A survey study, IEEE Access 11 (2023) 42431–42462.
[36] Sabine Paarmann, Markus Schreiber, Ahmed Chahbaz, Felix Hildenbrand, Gereon Stahl, Marcel Rogge, Philipp Dechent, Oliver Queisser, Sebastian Dominic Frankl, Pablo Morales Torricos, et al., Short-term tests, long-term predictions–accelerating ageing characterisation of lithium-ion batteries, Batter. Supercaps 7 (11) (2024) e202300594.
[37] Matthew Beatty, Dani Strickland, Pedro Ferreira, A review of methods of generating incremental capacity–differential voltage curves for battery health determination, Energies 17 (17) (2024) 4309.
[38] Wenxuan Hu, Yufan Peng, Yimin Wei, Yong Yang, Application of electrochemical impedance spectroscopy to degradation and aging research of lithium-ion batteries, J. Phys. Chem. C 127 (9) (2023) 4465–4495.
[39] Alexandros Ch Lazanas, Mamas I. Prodromidis, Electrochemical impedance spectroscopy–a tutorial, ACS Meas. Sci. Au 3 (3) (2023) 162–193.
[40] Bernard A. Boukamp, A linear Kronig-Kramers transform test for immittance data validation, J. Electrochem. Soc. 142 (6) (1995) 1885.
[41] Markos Koseoglou, Evangelos Tsioumas, Dimitrios Papagiannis, Nikolaos Jabbour, Christos Mademlis, A novel on-board electrochemical impedance spectroscopy system for real-time battery impedance estimation, IEEE Trans. Power Electron. 36 (9) (2021) 10776–10787.
[42] Jun Huang, Zhe Li, Jianbo Zhang, Dynamic electrochemical impedance spectroscopy reconstructed from continuous impedance measurement of single frequency during charging/discharging, J. Power Sources 273 (2015) 1098–1102.
[43] Noël Hallemans, Widanalage Dhammika Widanage, Xinhua Zhu, Sanghamitra Moharana, Muhammad Rashid, Annick Hubin, John Lataire, Operando electrochemical impedance spectroscopy and its application to commercial Li-ion batteries, J. Power Sources 547 (2022) 232005.
[44] Mohamed Massaoudi, Haitham Abu-Rub, Ali Ghrayeb, Advancing lithium-ion battery health prognostics with deep learning: A review and case study, IEEE Open J. Ind. Appl. 5 (2024) 43–62.
[45] Ruohan Guo, Weixiang Shen, A review of equivalent circuit model based online state of power estimation for lithium-ion batteries in electric vehicles, Vehicles 4 (1) (2021) 1–29.
[46] Brian OSPINA AGUDELO, Walter Zamboni, Monmasson Eric, Giovanni Spagnuolo, et al., Identification of battery circuit model from EIS data, in: Proceedings of the Jeunes Chercheurs En Genie Electrique (JCGE) Conference, 2019, pp. 1–6.
[47] Félix-A LeBel, Pascal Messier, Ali Sari, João Pedro F Trovão, Lithium-ion cell equivalent circuit model identification by galvanostatic intermittent titration technique, J. Energy Storage 54 (2022) 105303.
[48] Islam Md Monirul, Li Qiu, Rukhsana Ruby, Accurate SOC estimation of ternary lithium-ion batteries by HPPC test-based extended Kalman filter, J. Energy Storage 92 (2024) 112304.
[49] Woosung Choi, Heon-Cheol Shin, Ji Man Kim, Jae-Young Choi, Won-Sub Yoon, Modeling and applications of electrochemical impedance spectroscopy (EIS) for lithium-ion batteries, J. Electrochem. Sci. Technol. 11 (1) (2020) 1–13.
[50] Michael Schönleber, Dino Klotz, E. Ivers-Tiffée, A method for improving the robustness of linear Kramers-Kronig validity tests, Electrochim. Acta 131 (2014) 20–27.
[51] Matteo Galeotti, Lucio Cinà, Corrado Giammanco, Aldo Di Carlo, Francesco Santoni, Alessio De Angelis, Antonio Moschitta, Paolo Carbone, LiPo batteries dataset: Capacity, electrochemical impedance spectra, and fit of equivalent circuit model at various states-of-charge and states-of-health, Data Brief 50 (2023) 109561.
[52] Matteo Galeotti, Lucio Cinà, Corrado Giammanco, Aldo Di Carlo, Francesco Santoni, Alessio De Angelis, Antonio Moschitta, Paolo Carbone, LiPo battery LP-503562-IS-3 EIS, capacity, ECM data, 2023, http://dx.doi.org/10.17632/stcppt2r68.1.
[53] Thomas F. Coleman, Yuying Li, An interior trust region approach for nonlinear minimization subject to bounds, SIAM J. Optim. 6 (2) (1996) 418–445.

[54] Oskar Theliander, Anton Kersten, Manuel Kuder, Weiji Han, Emma Arfa Grunditz, Torbjorn Thiringer, Battery modeling and parameter extraction for drive cycle loss evaluation of a modular battery system for vehicles based on a cascaded H-bridge multilevel inverter, IEEE Trans. Ind. Appl. 56 (6) (2020) 6968–6977.
[55] Brian OSPINA AGUDELO, Walter Zamboni, Eric Monmasson, Giovanni Spagnuolo, et al., Identification of battery circuit model from EIS data, in: Proceedings of the Jeunes Chercheurs En Genie Electrique (JCGE) Conference, 2019, pp. 1–6.
[56] Mohammad H Nadimi-Shahraki, Shokooh Taghian, Seyedali Mirjalili, An improved grey wolf optimizer for solving engineering problems, Expert Syst. Appl. 166 (2021) 113917.
[57] Yong Yu, Xiaosheng Si, Changhua Hu, Jianxun Zhang, A review of recurrent neural networks: LSTM cells and network architectures, Neural Comput. 31 (7) (2019) 1235–1270.
[58] Shiva Nosouhian, Fereshteh Nosouhian, Abbas Kazemi Khoshouei, A review of recurrent neural network architecture for sequence learning: Comparison between LSTM and GRU, 2021.
[59] Laith Alzubaidi, Jinglan Zhang, Amjad J Humaidi, Ayad Al-Dujaili, Ye Duan, Omran Al-Shamma, José Santamaría, Mohammed A Fadhel, Muthana Al-Amidie, Laith Farhan, Review of deep learning: concepts, CNN architectures, challenges, applications, future directions, J. Big Data 8 (2021) 1–74.
[60] Li Yang, Abdallah Shami, On hyperparameter optimization of machine learning algorithms: Theory and practice, Neurocomputing 415 (2020) 295–316.
[61] Bobak Shahriari, Kevin Swersky, Ziyu Wang, Ryan P Adams, Nando De Freitas, Taking the human out of the loop: A review of Bayesian optimization, Proc. IEEE 104 (1) (2015) 148–175.
[62] Justin B. Kinney, Gurinder S. Atwal, Equitability, mutual information, and the maximal information coefficient, Proc. Natl. Acad. Sci. 111 (9) (2014) 3354–3359.
[63] Spyridon Giazitzis, Maciej Sakwa, Sonia Leva, Emanuele Ogliari, Susheel Badha, Filippo Rosetti, A case study of a tiny machine learning application for battery state-of-charge estimation, Electron. 13 (10) (2024) 1964.
[64] Spyridon Giazitzis, Maciej Sakwa, Emanuele Ogliari, Susheel Badha, Filippo Rosetti, Tiny machine learning for li-ion battery state of health estimation, in: 2024 IEEE 22nd Mediterranean Electrotechnical Conference, MELECON, IEEE, 2024, pp. 1019–1024.
[65] Yuqin Weng, Wenkai Guan, Cristinel Ababei, Prediction of remaining useful life and cell temperature for li-ion batteries using TinyML, in: 2024 IEEE 67th International Midwest Symposium on Circuits and Systems, MWSCAS, IEEE, 2024, pp. 562–566.
[66] Song Han, Huizi Mao, William J. Dally, Deep compression: Compressing deep neural networks with pruning, trained quantization and huffman coding, 2015, arXiv preprint arXiv:1510.00149.
[67] Miguel A. Carreira-Perpinán, Yerlan Idelbayev, "Learning-compression" algorithms for neural net pruning, in: Proceedings of the IEEE Conference on Computer Vision and Pattern Recognition, 2018, pp. 8532–8541.
[68] Panagiotis Eleftheriadis, Spyridon Giazitzis, Sonia Leva, Emanuele Ogliari, Transfer learning techniques for the lithium-ion battery state of charge estimation, IEEE Access (2023).
[69] GitHub - tensorflow/tflite-micro: Infrastructure to enable deployment of ML models to low-power resource-constrained embedded targets.